Electronic Supplementary Information

Ab initio GGA+U Study of Oxygen Evolution and Oxygen Reduction Electrocatalysis on the (001) Surfaces of Lanthanum Transition Metal Perovskites $LaBO_3$ (B=Cr, Mn, Fe, Co and Ni)

Yueh-Lin LEE[1], Milind J. GADRE[4], Yang SHAO-HORN[*1,2,3], Dane MORGAN[4*]

[1]Electrochemical Energy Laboratory, [2]Department of Materials Science and Engineering, [3]Department of Mechanical Engineering, Massachusetts Institute of Technology, Cambridge, Massachusetts 02139, United States

[4]Department of Materials Science and Engineering, University of Wisconsin-Madison, Madison, Wisconsin 53706, United States

Index **Page**

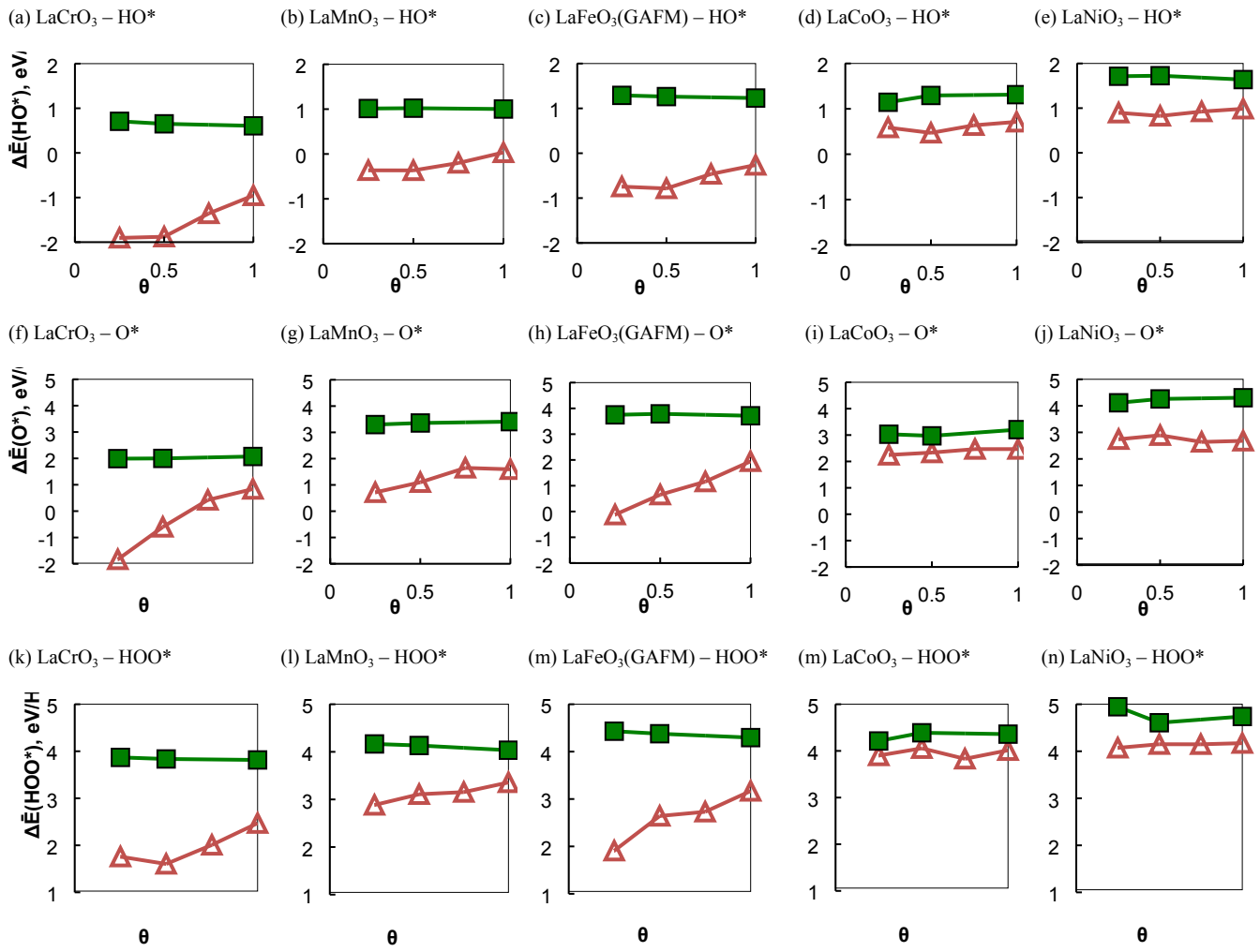
(a) LaCrO3 – HO*
(b) LaMnO3 – HO*
(c) LaFeO3(GAFM) – HO*
(d) LaCoO3 – HO*
(e) LaNiO3 – HO*
ΔĒ(HO*), eV/
(f) LaCrO3 – O*
(g) LaMnO3 – O*
(h) LaFeO3(GAFM) – O*
(i) LaCoO3 – O*
(j) LaNiO3 – O*
ΔĒ(O*), eV/
(k) LaCrO3 – HOO*
(l) LaMnO3 – HOO*
(m) LaFeO3(GAFM) – HOO*
(m) LaCoO3 – HOO*
(n) LaNiO3 – HOO*
ΔĒ(HOO*), eV/H
θ

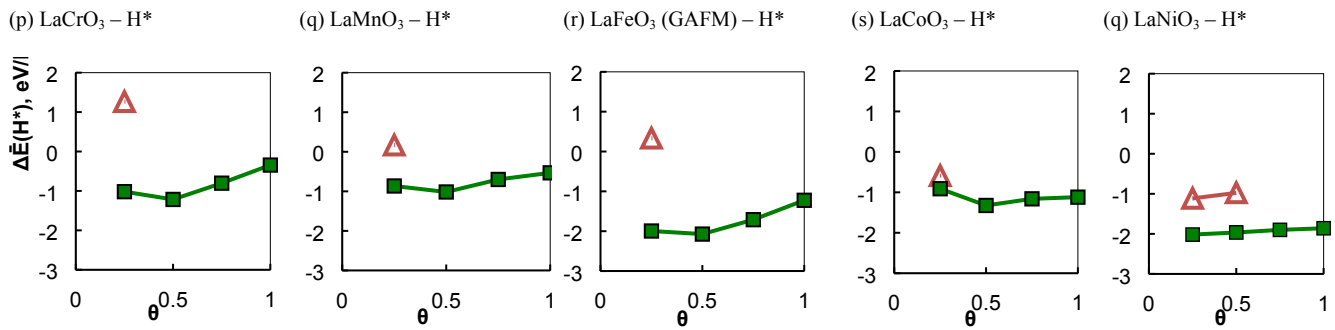

Figure S1. Top panel - perovskite (001) BO_2 (green squares, same below) and AO (red triangles, same below) HO* surface adsorption energy, ΔE(HO*), vs. surface coverage per (1×1) surface area for (a) $LaCrO_3$ (b) $LaMnO_3$ (c) $LaFeO_3$ (G-type AFM), (d) $LaCoO_3$ and (e) $LaNiO_3$. Second panel - perovskite (001) surface O* adsorption energy, ΔE(O*), vs. surface coverage per (1×1) surface area for (f) $LaCrO_3$ (g) $LaMnO_3$ (h) $LaFeO_3$ (G-type AFM), (i) $LaCoO_3$ and (j) $LaNiO_3$. Third panel - perovskite (001) surface HOO* adsorption energy, ΔE(HOO*), vs. surface coverage per (1×1) surface area for (k) $LaCrO_3$ (l) $LaMnO_3$ (m) $LaFeO_3$ (G-type AFM), (n) $LaCoO_3$ and (o) $LaNiO_3$. Bottom panel - perovskite (001) surface H* adsorption energy, ΔE(H*), vs. surface coverage per (1×1) surface area for (p) $LaCrO_3$ (q) $LaMnO_3$ (r) $LaFeO_3$ (G-type AFM), (s) $LaCoO_3$ and (t) $LaNiO_3$. Note that some H* data is not included in the bottom panel as the low-coverage data already showed the H* was not stable on the surface and would therefore play no role in the surface coverage effects.

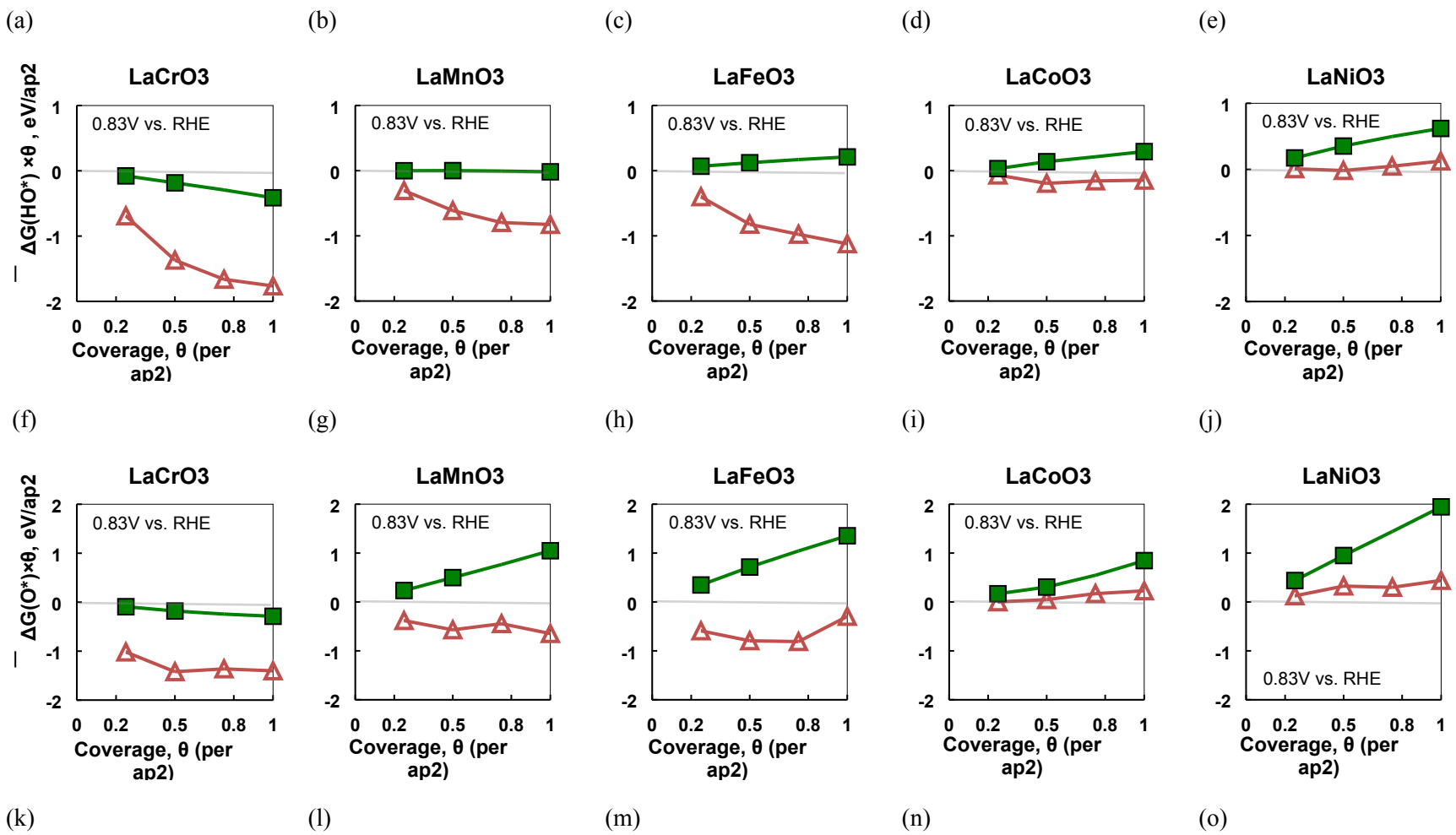
(a)
(b)
(c)
(d)
(e)
LaCrO3
LaMnO3
LaFeO3
LaCoO3
LaNiO3
0.83V vs. RHE
− ΔG(HO*) ×θ , eV/ap2
Coverage, θ (per ap2)
(f)
(g)
(h)
(i)
(j)
− ΔG(O*)×θ, eV/ap2
(k)
(l)
(m)
(n)
(o)

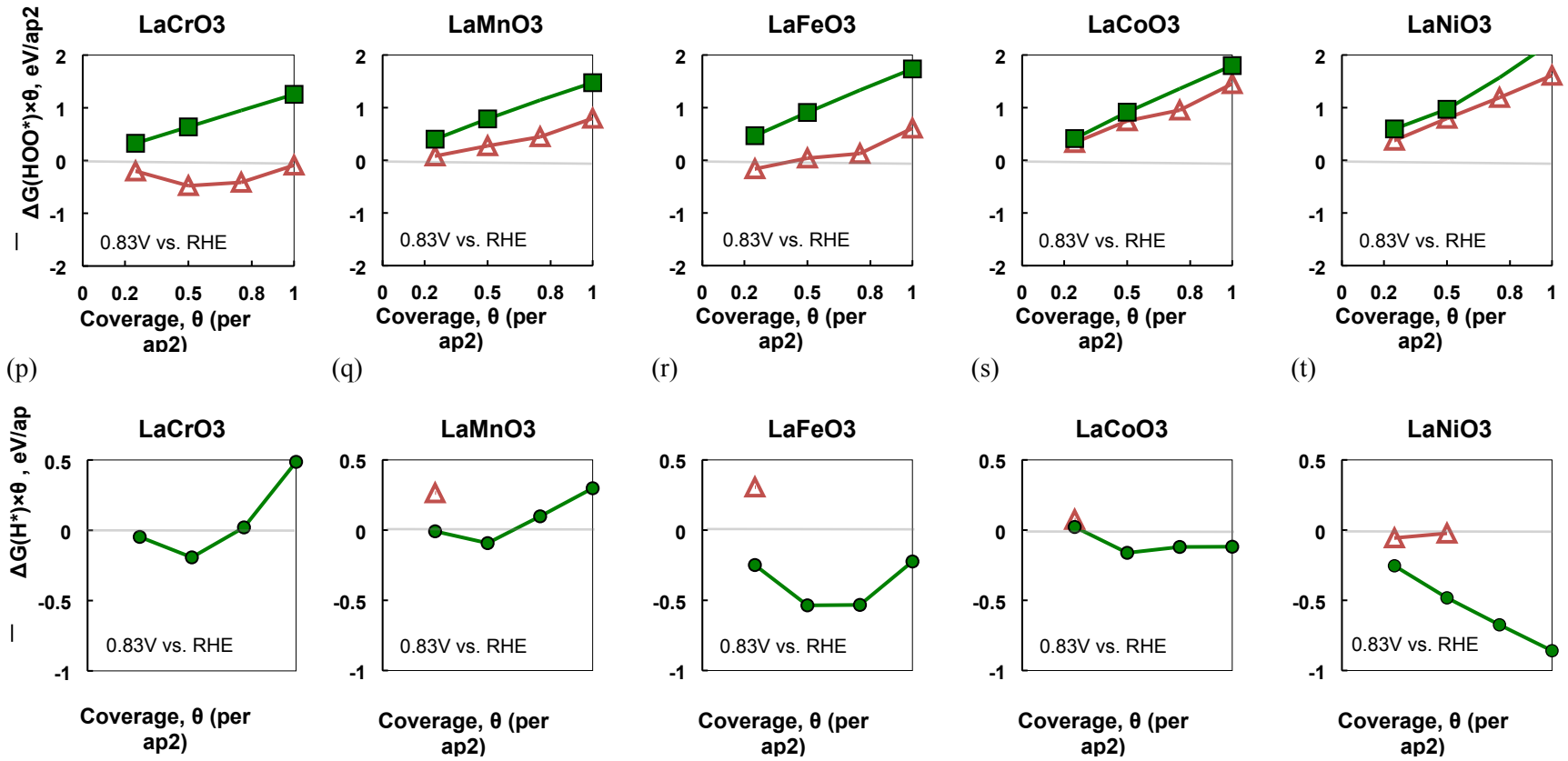

Figure S2. Top panel - perovskite (001) BO_2 (green squares, same below) and AO (red triangles, same below) HO* surface adsorption free energy per (1×1) surface area, *i.e.* surface adsorption free energy per adsorbate multiplied by surface coverage per (1×1) surface area, $\Delta\bar{G}$(HO*)×θ, vs. surface coverage per (1×1) surface area (a_p^2, where a_p is the perovskite (001) surface plane lattice constant) at 0.83 V vs. RHE for (a) $LaCrO_3$ (b) $LaMnO_3$ (c) $LaFeO_3$ (G-type AFM), (d) $LaCoO_3$ and (e) $LaNiO_3$. Second panel - perovskite (001) surface O* adsorption free energy per (1×1) surface area, $\Delta\bar{G}$(O*)×θ, vs. surface coverage per (1×1) surface area at 0.83 V vs. RHE for (f) $LaCrO_3$ (g) $LaMnO_3$ (h) $LaFeO_3$ (G-type AFM), (i) $LaCoO_3$ and (j) $LaNiO_3$. Third panel - perovskite (001) surface HOO* adsorption free energy per (1×1) surface area, $\Delta\bar{G}$(HOO*)×θ, vs. surface coverage per (1×1) surface area at 0.83 V vs. RHE for (k) $LaCrO_3$ (l) $LaMnO_3$ (m) $LaFeO_3$ (G-type AFM), (n) $LaCoO_3$ and (o) $LaNiO_3$. Bottom panel - perovskite (001) surface H* adsorption free energy per (1×1) surface area, $\Delta\bar{G}$(H*)×θ, vs. surface coverage per (1×1) surface area at 0.83 V vs. RHE for (p) $LaCrO_3$ (q) $LaMnO_3$ (r) $LaFeO_3$ (G-type AFM), (s) $LaCoO_3$ and (t) $LaNiO_3$. Note that some H* data is not included in the bottom panel as the low-coverage data already showed the H* was not stable on the surface and would therefore play no role in the surface coverage effects.

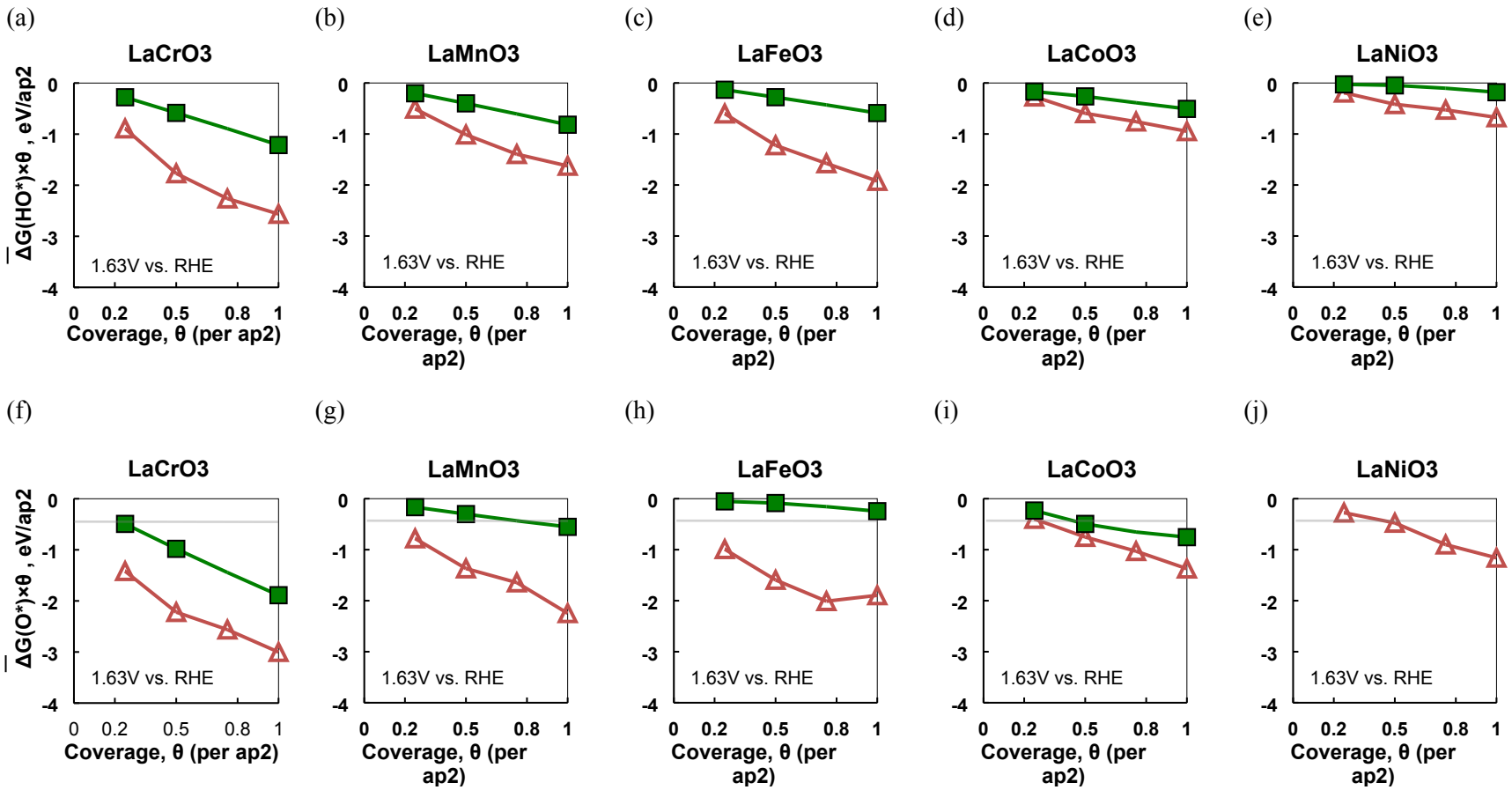
(a)
LaCrO3
(b)
LaMnO3
(c)
LaFeO3
(d)
LaCoO3
(e)
LaNiO3
(f)
LaCrO3
(g)
LaMnO3
(h)
LaFeO3
(i)
LaCoO3
(j)
LaNiO3
ΔG(HO*)×θ , eV/ap2
ΔG(O*)×θ , eV/ap2
0
-1
-2
-3
-4
0 0.2 0.5 0.8 1
Coverage, θ (per ap2)
1.63V vs. RHE

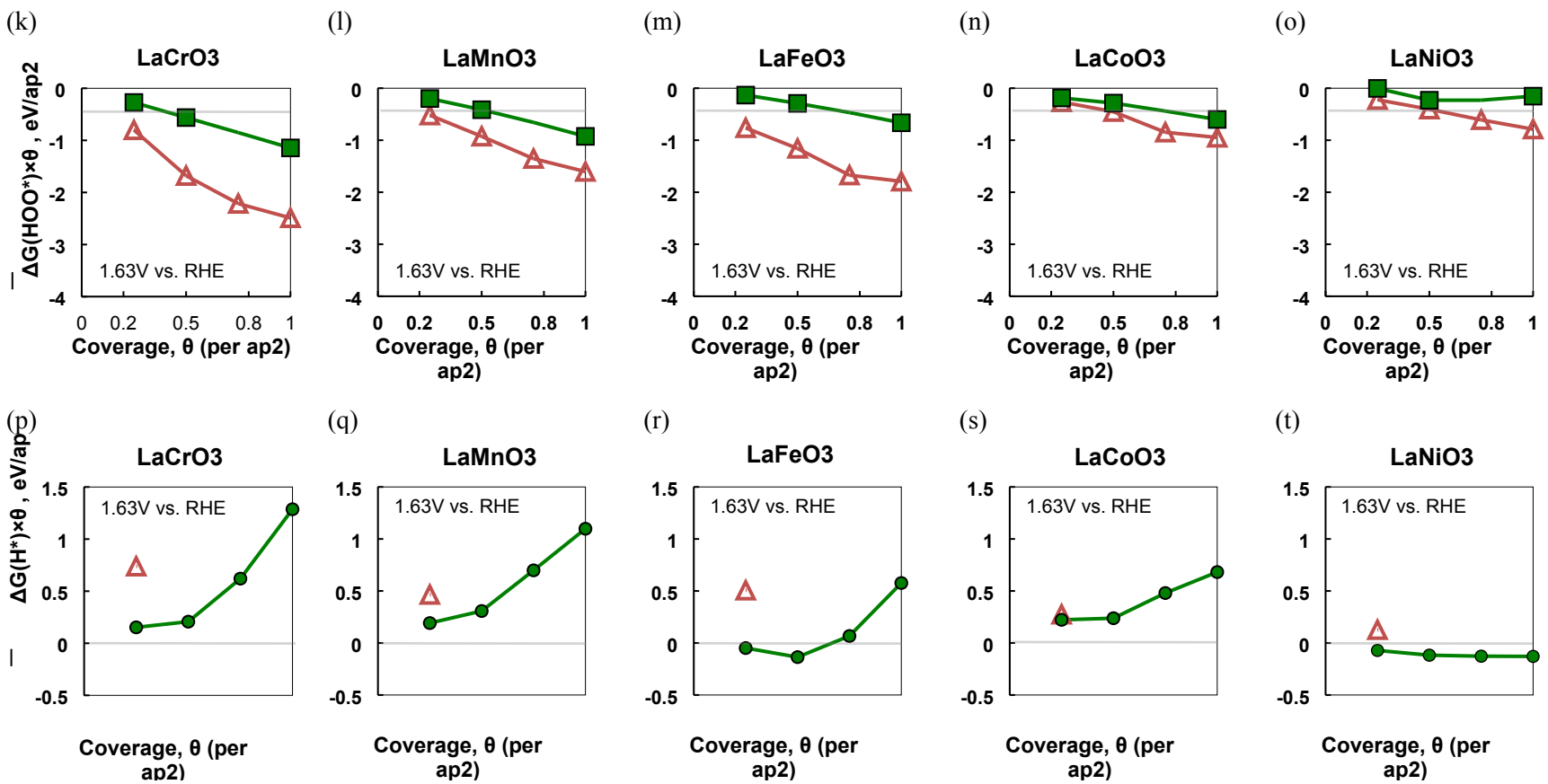

Figure S3. Top panel - perovskite (001) BO_2 (green squares, same below) and AO (red triangles, same below) HO* surface adsorption free energy per (1×1) surface area, *i.e.* surface adsorption free energy per adsorbate multiplied by surface coverage per (1×1) surface area, $\Delta\bar{G}$(HO*)×θ, vs. surface coverage per (1×1) surface area (a_p^2, where a_p is the perovskite (001) surface plane lattice constant) at 1.63 V vs. RHE for (a) $LaCrO_3$ (b) $LaMnO_3$ (c) $LaFeO_3$ (G-type AFM), (d) $LaCoO_3$ and (e) $LaNiO_3$. Second panel – perovskite (001) surface O* adsorption free energy per (1×1) surface area, $\Delta\bar{G}$(O*)×θ, vs. surface coverage per (1×1) surface area at 1.63 V vs. RHE for (f) $LaCrO_3$ (g) $LaMnO_3$ (h) $LaFeO_3$ (G-type AFM), (i) $LaCoO_3$ and (j) $LaNiO_3$. Third panel - perovskite (001) surface HOO* adsorption free energy per (1×1) surface area, $\Delta\bar{G}$(HOO*)×θ, vs. surface coverage per (1×1) surface area at 1.63 V vs. RHE for (k) $LaCrO_3$ (l) $LaMnO_3$ (m) $LaFeO_3$ (G-type AFM), (n) $LaCoO_3$ and (o) $LaNiO_3$. Bottom panel - perovskite (001) surface H* adsorption free energy per (1×1) surface area, $\Delta\bar{G}$(H*)×θ, vs. surface coverage per (1×1) surface area at 1.63 V vs. RHE for (p) $LaCrO_3$ (q) $LaMnO_3$ (r) $LaFeO_3$ (G-type AFM), (s) $LaCoO_3$ and (t) $LaNiO_3$. The free energy of H* adsorption at 1.63 V vs. RHE was found to be all positive for the (001) AO surfaces of the investigated perovskites and therefore, the $\Delta\bar{G}$(H*)×θ for the H* adsorption on the (001) AO surfaces is neglected in plots (p)~(t). Note that some H* data is not included in the bottom panel as the low-coverage data already showed the H* was not stable on the surface and would therefore play no role in the surface coverage effects.

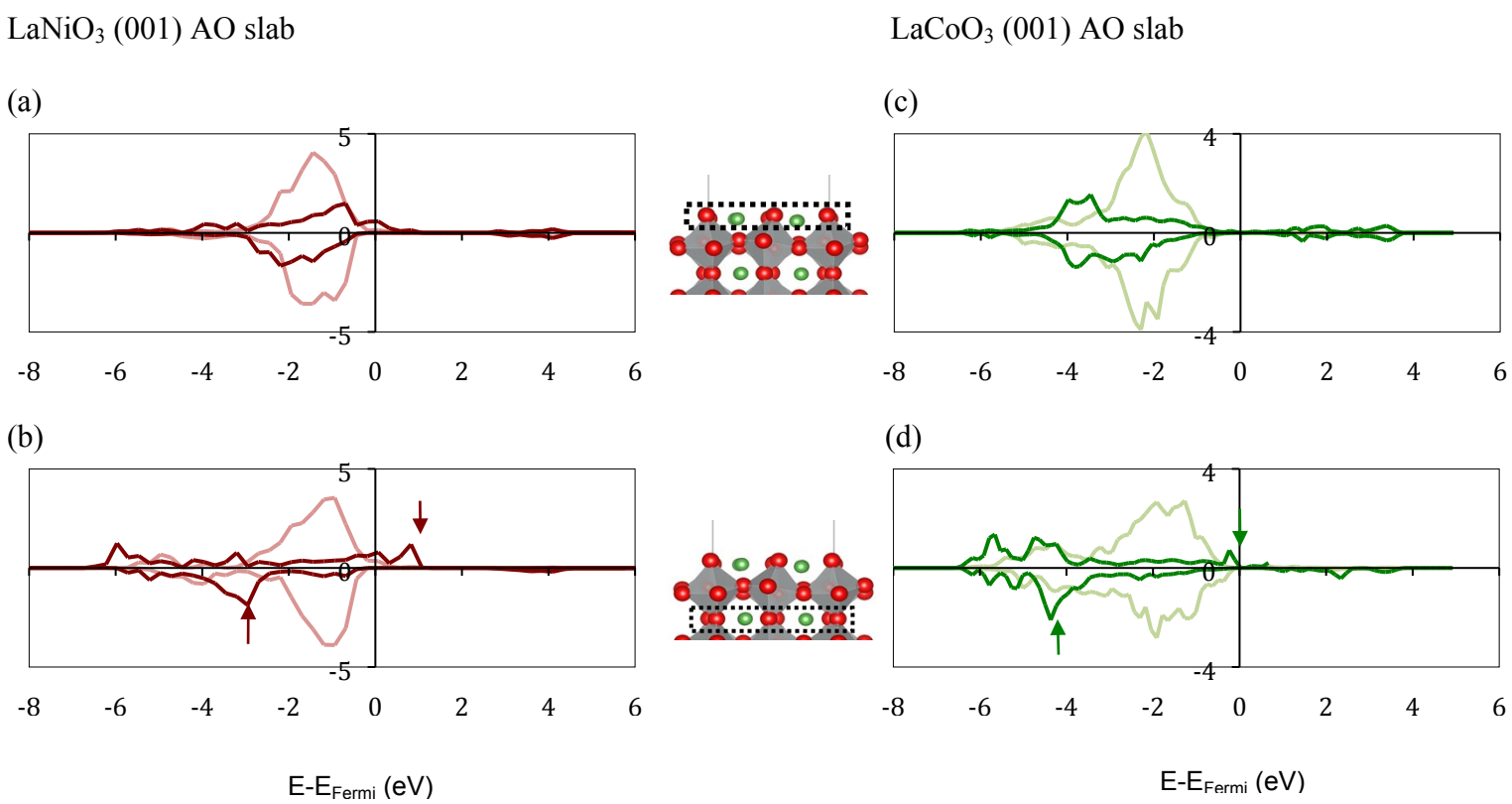

Figure S4. (a) $LaNiO_3$ ideal (001) AO slab top surface layer oxygen project density of states (b) $LaNiO_3$ ideal (001) AO slab third layer oxygen project density of states (c) $LaCoO_3$ ideal (001) AO slab top surface layer oxygen project density of states and (d) $LaCoO_3$ ideal (001) AO slab third layer oxygen project density of states. The reference energy is aligned at the Fermi energy level. Schematics of the (001) AO slab layers are provided with dashed squares to show the indicated oxygens. The oxygen p_z states, which strongly hybridize with transition metal 3*d* states, are shown by the deep-color lines, while the oxygen $p_x + p_z$ states, which are less hybridized with the transition metal 3*d* states , are shown by the light-color lines. Arrows in the projected density of state plots represent transition metal 3*d*-oxygen p_z bonding (up-arrow) and anit-bonding (down-arrow) states.

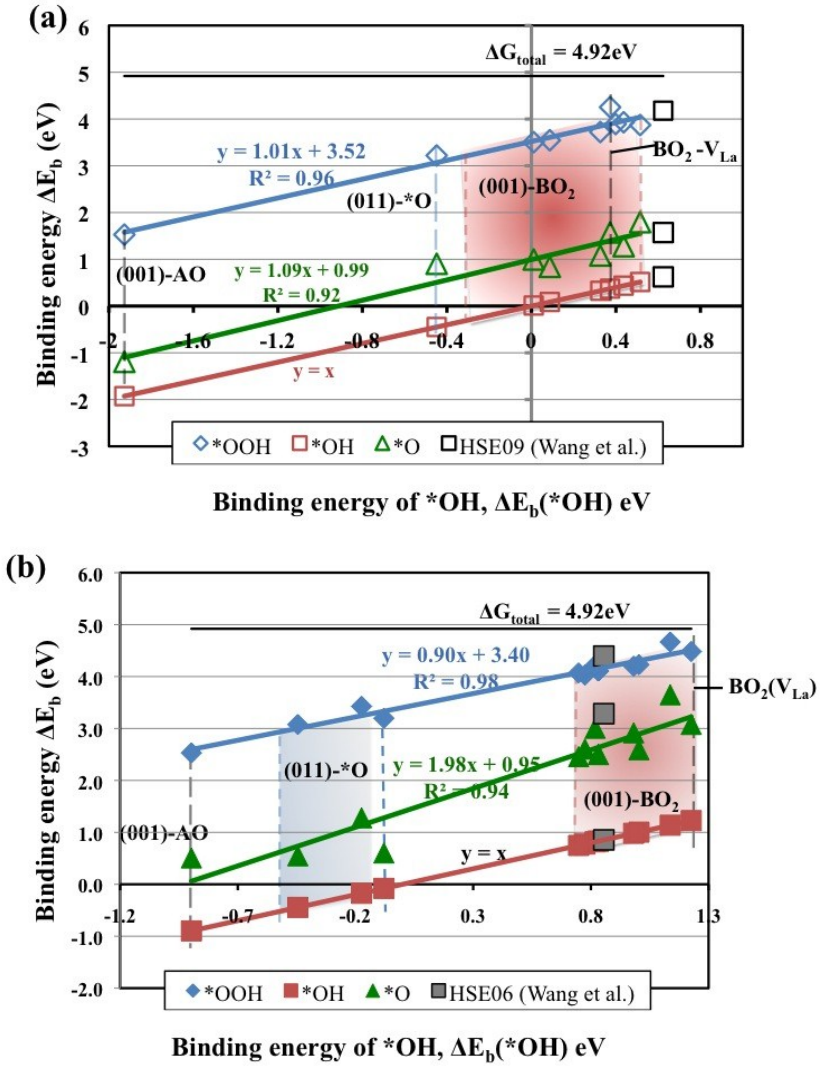

Figure S5: Scaling relations for the binding energies of reactive intermediates of ORR and OER on (a) $LaCrO_3$ and (b) $LaMnO_3$ surfaces. Binding energies > 0 mean energy is gained in binding to the surface. Binding energies are for *OOH *(blue diamonds), *O (green triangles) and *OH (red squares) on y-axis, as a function of binding energy of *OH on the x-axis. (a) Binding energies of reactive intermediates of ORR and OER (*O, *OH, *OOH) for $LaCrO_3$ as a function of the *OH binding energy at 0V (RHE). Data points for HSE06 (blue squares) are referred from Wang *et al*.[1]. OH and OOH binding energies approximately scale as ΔE(*OOH)=ΔE(*OH)+3.52eV. Shaded region denotes the set of different binding energies for a range of surfaces of (001)-BO_2 terminated $LaCrO_3$. (b) Binding energies of reactive intermediates of ORR and OER (*O, *OH, *OOH) for $LaMnO_3$ as a function of the *OH binding energy at 0V (RHE). Data points for HSE06 are referred from Wang et al.[1]. OH and OOH binding energies approximately scale as ΔE(*OOH)= ΔE(*OH)+3.40 eV. Blue and red shaded regions denote the set of different binding energies for a range of surfaces of (011)-O-terminated and (001)-BO_2 terminated $LaMnO_3$. Binding energies are given for bare and covered surfaces.

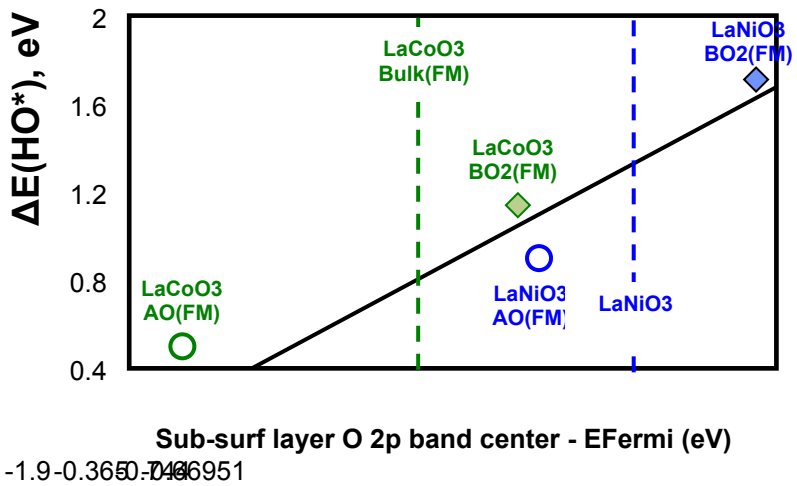

Figure S6. The calculated ΔE(HO*) vs the sub-surface layer O 2p band center relative to the Fermi level (the second slab layer beneath the surface termination) of $LaCoO_3$-FM (green symbols) and $LaNiO_3$-FM (blue symbols) (001) AO (empty circles) and BO_2 (filled diamonds) slabs. The dashed line represents the computed bulk $LaCoO_3$-FM and $LaNiO_3$-FM O-2p band centers taken from Ref.[2]. The figure demonstrates the opposite surface band bending between the (001) AO and BO_2 surfaces with respect to the bulk leads to the distinct surface ΔE(HO*) adsorption energies.

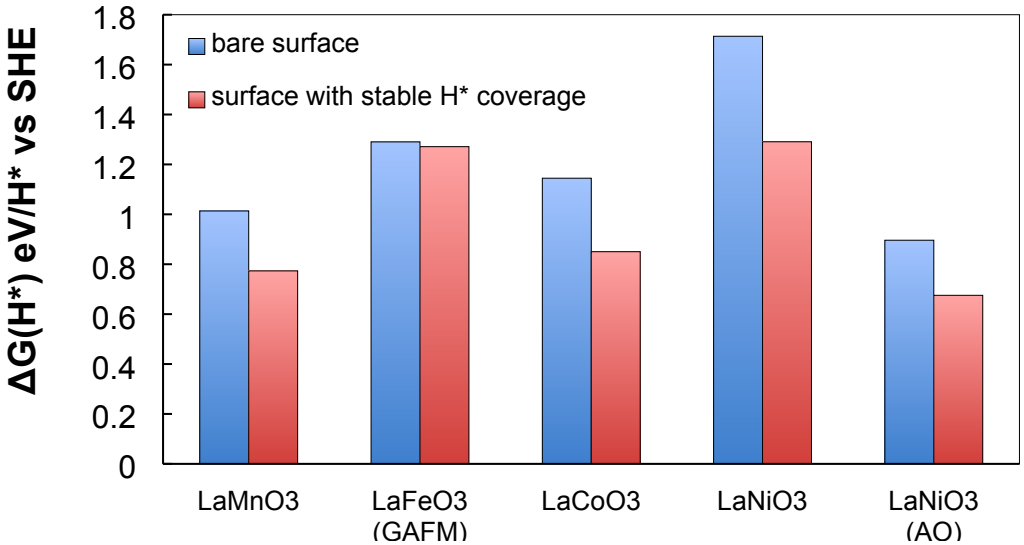

Figure S7: A comparison of the HO* adsorption energy (eV/HO*) vs. SHE simulated at the low coverage limit (0.25ML) between the bare (in blue) and stable H* covered (in red) for $LaMnO_3$, $LaFeO_3$ (GAFM), $LaCoO_3$, and $LaNiO_3$ (001) BO_2 surfaces as well as $LaNiO_3$ (001) AO surfaces (labeled as $LaNiO_3$ (AO)). The H* covered surfaces were predicted to be the stable (001) BO_2 surfaces at applied potential of 0.83 V vs. RHE for $LaMnO_3$ (0.5 ML H*), $LaFeO_3$ (GAFM) (0.5 ML H*), $LaCoO_3$ (0.5 ML H*), $LaNiO_3$ (1ML H*) while the $LaNiO_3$ (001) AO surfaces was shown to be stable with 0.25 ML H* (see Table 2, Figure S2, and Figure 3).

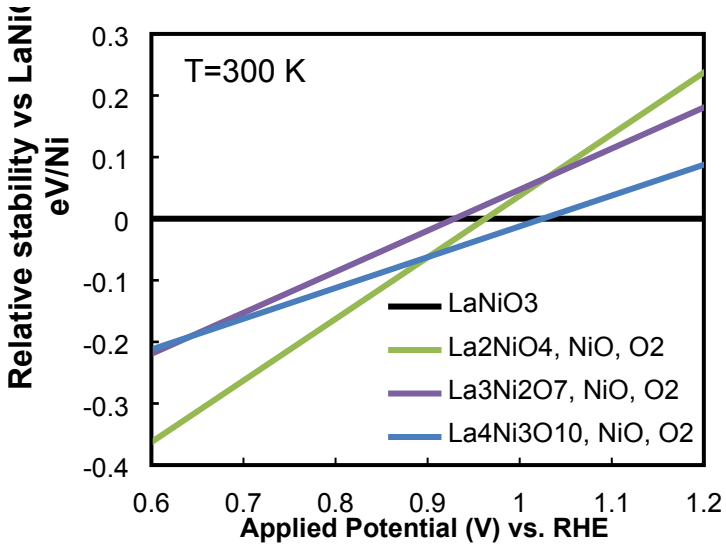

Figure S8. GGA+U bulk stability calculations for $LaNiO_3$ relative to the reactions of forming Ruddelsden-Popper phase $La_{n+1}Ni_nO_{3n+1}$ (with NiO and O_2). Our results suggest the instability of $LaNiO_3$ under the ORR conditions (shaded area) to form the Ruddelsden-Popper phase.

References:

1. Wang, Y. and H.-P. Cheng, *Oxygen Reduction Activity on Perovskite Oxide Surfaces: A Comparative First-Principles Study of LaMnO3, LaFeO3, and LaCrO3.* The Journal of Physical Chemistry C, 2013. **117**(5): p. 2106-2112.
2. Lee, Y.-L., et al., *Prediction of solid oxide fuel cell cathode activity with first-principles descriptors.* Energy & Environmental Science, 2011. **4**(10): p. 3966-3970.